Higher order harmonics of modulational instability

David Amans,[1] Edouard Brainis,[2] and Serge Massar[3]
[1]*Institut de Microélectronique, Electromagnétisme et Photonique, ENSERG, 23 avenue des martyrs, Boite Postale 257, 38016 Grenoble, France*
[2]*Optique et Acoustique, C.P. 194/5, Université Libre de Bruxelles, Avenue F. D. Roosevelt 50, 1050 Bruxelles, Belgium*
[3]*Laboratoire d'Information Quantique and QUIC, Université Libre de Bruxelles, C.P. 165/59, Avenue F. D. Roosevelt 50, 1050 Bruxelles, Belgium*
(Received 16 March 2005; revised manuscript received 27 July 2005; published 28 December 2005)

We study the higher order harmonics of scalar modulational instability in the regime where it arises spontaneously through amplification of vacuum fluctuations. We obtain detailed predictions concerning the detunings, intensities, growth rates, and spectral widths of the harmonics. These predictions are well verified by experimental results obtained by propagating high intensity light pulses through optical fibers.

DOI: 10.1103/PhysRevE.72.066617 PACS number(s): 42.81.−i, 05.45.−a, 42.65.Ky

I. INTRODUCTION

In a nonlinear dispersive medium the propagation of a continuous wave may be impeded by the phenomenon of modulational instability (MI) whereby the continuous wave breaks up into a train of localized pulses. This effect has been predicted and verified in many branches of physics, including fluid dynamics [1], plasma physics [2], nonlinear optics [3–6], and Bose-Einstein condensates [7].

In the spectral domain the instability induces the appearance of new frequencies whose amplitude grows exponentially. As the dynamical process continues more and more energy is converted from the monochromatic wave to the sidebands. Simultaneously harmonics of the unstable frequencies appear and also grow exponentially.

Although the process of MI is by now textbook material, the subsequent dynamics, and in particular the appearance of the higher harmonics, has been relatively little studied. The main work we are aware about in this context is theoretical [8] and experimental [9] investigations in the context of the Fermi-Pasta-Ulam recurrence. It is important to note that in these works the initial noise was taken to be a classical wave at a specific frequency and the analysis therefore involves a discrete set of modes.

In the present work we study both theoretically and experimentally the growth of the higher order harmonics of MI in the regime where the instability arises by spontaneous amplification of vacuum fluctuations. The essential difference with respect to the earlier work mentioned above is that in the present case a continuous spectrum of vacuum fluctuations is involved (rather than a discrete set of modes). We will characterize each harmonic by its detuning, its intensity and growth rate, and its spectral width. Several of these features would be different, or would simply not appear (in the case of the spectral width), if one was dealing with a discrete set of modes.

Our investigation is carried out in the regime of large gain, when many photons have been created in the sidebands, but before we reach the regime of pump depeletion (i.e., before the energy in the sidebands becomes comparable to the energy in the initial monochromatic wave). One of the main interests of our work is to show how, even though we are working in a semiclassical regime where many photons are produced, the fact that the instability is seeded by vacuum flucutations leaves a distinct signature in the spectrum of the sidebands.

Our analytical predictions are well reproduced in our experimental demonstration, based on light propagation through optical fibers. This system is particularly well suited for such investigations because light propagation in low loss silica fibers is accurately described by the nonlinear Schrödinger equation (NLSE) and hence suitable for precise theoretical modeling, and because it is fairly easy to work in a regime where initial noise is dominated by vacuum fluctuations. In fact the appearance of the first harmonic—probably seeded by vacuum fluctuations—was already reported in the first experimental investigation of MI in optical fibers [5]. Thus our approach provides quantitative explanation for the complex spectra—readily observable in experiments—that arise in MI seeded by vacuum fluctuations in the regime of large gain. A related comparison, but between numerical simulations and experimental results, can be found in [10].

Finally we note that the ideas and methods developed here are not restricted to the problem of scalar MI, but should apply with appropriate changes to other forms of MI such as vectorial MI, and more generally to any unstable dynamical system involving a continuous set of modes (i.e., described by partial differential equations), when the instability is seeded by vacuum fluctuations. We also note that our analysis can also be applied if the initial noise is classical white noise.

Section II A contains our theoretical analysis. Our key result is Eq. (16) which encapsulates our predictions concerning intensities, growth rates, frequencies, and spectral widths of the harmonics. A discussion of the predictions provided by Eq. (16), of the hypotheses that go into its derivation, and of its interpretation, are given in Sec. II B. Some background material, and details of some calculations have been relegated to Appendixes. Section III describes our experimental setup and shows that the experimental results are in good agreement with the theoretical predictions.

II. THEORETICAL ANALYSIS

A. Harmonics of modulational instability

Let $A(x,\tau)$ be the slowly varying field envelope of a light pulse propagating in an isotropic single mode fiber with carrier frequency ω_0, where x is the coordinate along the fiber and $\tau=t-x/v_g$ is the time variable of coordinates moving at group velocity v_g. It obeys the NLSE (see Ref. [6])

$$i\partial_x A = \frac{\beta_2}{2}\partial_\tau^2 A - \gamma|A|^2 A, \tag{1}$$

where β_2 is the group velocity dispersion at frequency ω_0 and $\gamma=2n_2\omega_0/\epsilon_0 c^2 n_0 A_{eff}$ with n_0 the effective linear refraction index for light guided in the fiber, n_2 the nonlinear refraction index, and A_{eff} the effective cross section of the fiber. With this normalization $|A(x,\tau)|^2$ is the instantaneous power flowing through the fiber at position x at time τ.

We take the unperturbed solution to be

$$A = A_0 e^{i\phi_{NL}} \tag{2}$$

with A_0 a constant and $\phi_{NL}=\gamma A_0^2 x$ the nonlinear phase. As is well known, when $\beta_2<0$ (the anomalous dispersion regime), the continuous solution Eq. (2) is unstable. We give the "standard" derivation of this instability (following [6]) in Appendix A, where we also include the predictions of quantum theory (when the instability is seeded by vacuum fluctuations) and discuss the regime of large gain.

In the present article we use a slightly different approach inspired by work of Hasegawa and Brinkman [4]. This will allow us to derive many of the properties of the harmonics of MI (which are inaccessible using the standard method of Appendix A).

Our starting point is to parametrize the solution as

$$A(x,\tau) = A_0 e^{i\phi_{NL}}[1+\epsilon(x,\tau)]^{1/2} e^{i\sigma(x,\tau)}, \tag{3}$$

where ϵ and σ are real variables. Upon insertion of this ansatz into the NLSE one obtains the equations

$$\frac{\partial_x \epsilon}{1+\epsilon} - \beta_2\left(\frac{\partial_\tau\sigma\,\partial_\tau\epsilon}{1+\epsilon} + \partial_\tau^2\sigma\right) = 0,$$

$$\frac{\beta_2}{2}\left(\frac{(\partial_\tau\epsilon)^2}{4(1+\epsilon)^2} - \frac{\partial_\tau^2\epsilon}{2(1+\epsilon)} + (\partial_\tau\sigma)^2\right) - \partial_x\sigma + \gamma|A_0|^2\epsilon = 0. \tag{4}$$

The key to the approach of Hasegawa and Brinkman is to keep the nonlinear dependence of A in ϵ and σ in Eq. (3), but to linearize Eqs. (4). Obviously this does not provide an exact solution to the NLSE, nor does it provide a consistent way to expand the solution, but it yields an approximate solution which captures many of the features of an exact solution (illustrated for instance by the good agreement between these theoretical predictions and our experimental results). This approach may, however, induce systematic errors that could grow with the order of the harmonics. We discuss the limitations of this approach in detail in Sec. II B.

Upon linearization of Eqs. (4) one obtains the following simplified set of equations:

$$\partial_x\epsilon - \beta_2\partial_\tau^2\sigma = 0, \quad -\partial_x\sigma - \frac{\beta_2}{4}\partial_\tau^2\epsilon + \gamma|A_0|^2\epsilon = 0. \tag{5}$$

The Fourier transforms of ϵ and σ are

$$\epsilon(x,\tau) = \frac{1}{\sqrt{2\pi}}\int_0^\infty d\omega\ \epsilon(x,\omega)e^{-i\omega\tau} + \epsilon^*(x,\omega)e^{+i\omega\tau},$$

$$\sigma(x,\tau) = \frac{1}{\sqrt{2\pi}}\int_0^\infty d\omega\ \sigma(x,\omega)e^{-i\omega\tau} + \sigma^*(x,\omega)e^{+i\omega\tau}. \tag{6}$$

When $\beta_2<0$ and $0<\omega^2<4\gamma A_0^2/|\beta_2|$ these equations possess exponentially growing solutions

$$\epsilon(x,\omega) = \epsilon_+(\omega)e^{gx} + \epsilon_-(\omega)e^{-gx},$$

$$\sigma(x,\omega) = \frac{g}{\omega^2|\beta_2|}\epsilon_+(\omega)e^{gx} - \frac{g}{\omega^2|\beta_2|}\epsilon_-(\omega)e^{-gx}, \tag{7}$$

where

$$g = \frac{|\beta_2|\omega}{2}\left(\frac{4\gamma A_0^2}{|\beta_2|} - \omega^2\right)^{1/2}. \tag{8}$$

As discussed in Appendix A one can also write the solution to the NLSE as

$$A(x,\tau) = e^{i\phi_{NL}}\left(A_0 + \frac{1}{\sqrt{2\pi}}\int d\omega\ a_\omega(x)e^{-i\omega\tau} + \text{c.c.}\right),$$

where a_ω are the positive frequency components of the initial noise. The importance of this decomposition is that in the quantum theory a_ω should be identified with the Heisenberg destruction operators. To obtain the relation between $\epsilon_\pm$ and a we linearize Eq. (3) to obtain

$$A = A_0 e^{i\phi_{NL}}(1+\epsilon/2+i\sigma)$$

and then compare the two solutions. The details of this comparison are given in Appendix B.

In the present work we are interested in the regime of large gain when $gx\gg 1$. This implies several simplifications. First we can neglect e^{-gx} with respect to e^{+gx}. Second we note that g has a maximum at

$$\omega_{max} = \sqrt{\frac{2\gamma}{|\beta_2|}}A_0; \tag{9}$$

hence we need its value only in the vicinity of ω_{max},

$$g(\omega) \simeq g_{max} - |\beta_2|(\omega-\omega_{max})^2 \tag{10}$$

with $g_{max}=\gamma A_0^2$. Finally all other functions can be approximated by their value at ω_{max} (since they do not appear in exponentials, but only as prefactors).

With these simplifications, Eqs. (7) lead to the following relation between σ and ϵ:

$$\sigma \simeq \frac{\epsilon}{2}, \tag{11}$$

and the relation between $\epsilon_\pm$ and a, derived in Eq. (B1), becomes

$$\epsilon \simeq \frac{1}{2A_0\sqrt{\pi}}\int_{\omega\simeq\omega_{max}} d\omega\, e^{-i\omega\tau+g(\omega)x}(a_\omega e^{-i\pi/4}+a^*_{-\omega}e^{i\pi/4})+\text{c.c.} \tag{12}$$

The condition that $gx \gg 1$ implies that many photons are created in the sidebands. Thus we can neglect quantum ordering problems and we can take a_ω to be classical white noise with moments

$$\langle a_{\omega_1}\cdots a_{\omega_n}a^*_{\omega'_1}\cdots a^*_{\omega'_m}\rangle = \frac{(\hbar\omega_0)^n}{2^n}\delta_{n,m} \times\sum_\sigma \delta(\omega_1-\omega'_{\sigma(1)})\cdots\delta(\omega_n-\omega'_{\sigma(n)}), \tag{13}$$

where the sum is over all permutations σ of $\{1,\ldots,n\}$.

In summary we have obtained an approximate solution of the NLSE

$$A \simeq A_0 e^{i\phi_{NL}}(1+\epsilon)^{1/2}e^{i\epsilon/2} \tag{14}$$

with ϵ given by Eq. (12) and a_ω classical white noise as described in Eq. (13).

In order to study the power spectrum of the harmonics, we expand Eq. (14) as a series in ϵ to obtain

$$A = A_0 e^{i\phi_{NL}}\sum_{n=0} c_n\epsilon^n, \tag{15}$$

where c_n are the Taylor series coefficients

$$c_n = \sum_{p=0}^{n}\frac{\Gamma_{n-p}(1/2)}{(n-p)\,!\,p!}\left(\frac{i}{2}\right)^p,$$

$$\Gamma_n(\alpha) = 1\times\alpha\times(\alpha-1)\cdots(\alpha-n+1),$$

the first few coefficients of which are

$$c_0=1,\quad c_1=\frac{1+i}{2},\quad c_2=\frac{-1+i}{4},\quad c_3=\frac{-i}{12},\quad c_4=\frac{-1+i}{48}.$$

Recall that ϵ contains the frequencies around both $+\omega_{max}$ and $-\omega_{max}$ [see Eq. (12)]. Hence ϵ^n contains frequencies around $n\omega_{max}$, $(n-2)\omega_{max}$, …, $-(n-2)\omega_{max}$, $-n\omega_{max}$. Thus each power in Eq. (15) gives rise to a new harmonic around frequencies $\pm n\omega_{max}$. Also there is a component around $\omega=0$ which first arises at order $n=2$.

To compute the power spectrum of these harmonics we take the Fourier transform at frequency $n\omega_{max}+\delta$ of the nth order term in Eq. (15):

$$A_n(n\omega_{max}+\delta) = \frac{1}{\sqrt{2\pi}}\int d\tau\, e^{i(n\omega_{max}+\delta)\tau}c_nA_0e^{i\phi_{NL}}\epsilon^n(\tau).$$

The spectral energy density at frequency $n\omega_{max}+\delta$ is

$$P_n(n\omega_{max}+\delta) = \langle|A_n(n\omega_{max}+\delta)|^2\rangle.$$

The computation of $P_n(n\omega_{max}+\delta)$ is somewhat tedious and details are given in Appendix B. The result of the computation is

$$P_n(n\omega_{max}+\delta) = \delta(0)\frac{(\hbar\omega_0)^n|c_n|^2\sqrt{n}(n-1)!}{|A_0|^{2(n-1)}2^{2n-1}(2\pi|\beta_2|x)^{(n-1)/2}} \times\exp(2ng_{max}x)\exp\left(-2|\beta_2|x\frac{\delta^2}{n}\right) \tag{16}$$

with $n=1, 2, 3, \ldots$, and the first few Taylor coefficients are $|c_0|^2=1$, $|c_1|^2=1/2$, $|c_2|^2=1/8$, $|c_3|^2=1/144$, $|c_4|^2=1/1152$.

The appearance of $\delta(0)$ should be interpreted as usual in this kind of calculation as $\delta(0)=T/2\pi$ with T the duration of the light pulse. Dividing by T yields the spectral power density.

For $n=1$ this describes the growth of the MI sidebands; and for $n>1$ it describes the growth of the harmonics. As mentioned above the first harmonic ($n=2$) also contains a component around $\omega=0$. One can repeat the above calculation to find that it is equal to $4P_2$, i.e., it has exactly the same shape as the first harmonic around $2\omega_{max}$ except that it is centered around $\omega=0$ and is four times more intense.

B. Summary of predictions and interpretation

Let us first summarize the main predictions contained in Eq. (16); we will then discuss the interpretation and limitations of our theoretical method. These predictions are as follows.

(1) We recover the well known result that the fundamental instability appears at frequency $\pm\omega_{max}=\pm\sqrt{2\gamma A_0^2/|\beta_2|}$, grows at a rate $2g_{max}=2\gamma|A_0|^2$, and has spectral width $\Delta\omega=\sigma_1=1/2\sqrt{|\beta_2|x}$.

(2) The power spectrum exhibits a series of Gaussian peaks centered on frequencies $n\omega_{max}$, $n=\ldots,-3,-2,-1,0,1,2,3,\ldots$ ($n=\pm1$ corresponds to the fundamental instability just mentioned).

(3) The $(n-1)$th harmonic appears at detuning $\omega_n=\pm n\omega_{max}$, grows at a rate $2g_n=2ng_{max}=2n\gamma|A_0|^2$, and has spectral width $\Delta\omega=\sigma_n=\sqrt{n}\sigma_1=\sqrt{n}/2\sqrt{|\beta_2|x}$.

In addition the first harmonic has a component around $\omega=0$ which has the same properties as the component around $2\omega_{max}$ except that its intensity is four times larger.

(4) Whereas the fundamental instability can be stimulated by a classical signal around the frequency ω_{max}, the harmonics cannot be stimulated. They are entirely determined by the initial noise around the frequency of the fundamental instability. We have verified this prediction experimentally by injecting a classical signal at frequency $2\omega_{max}$ and checking that it does not affect the power spectrum of the harmonics.

(5) The exact intensity of the harmonics is highly sensitive to any classical noise present initially around the frequency ω_{max} of the MI. Indeed the intensity of the $(n-1)$th harmonic will be multiplied by $(1/2+n_{class})^n$ where n_{class} is the number of classical noise photons per mode initially present. The sensitivity thus increases with the order of the harmonic.

The derivation of Eq. (16) raises a number of questions. First of all, the above analysis can be thought of as an expansion valid when there is no pump depletion, i.e., when the power in the modulational instability sidebands is small with respect to the power in the pump beam. When pump deple-

tion can no longer be neglected our computation is no longer valid, since we supposed that the pump amplitude is constant. Furthermore, in the regime where the pump gets depleted there will be a back action of the higher order harmonics on the lower order ones, an effect we neglected (for instance we considered only the contribution of A_n to P_n, and neglected the contributions of $A_{n'}$, $n' > n$).

The ratio η between the energy in the fundamental sidebands at frequency ω_{max} and $-\omega_{max}$, and the pump energy can be explicitly computed to be

$$\eta = 2\frac{\int d\delta\, P_1(\omega_{max}+\delta)}{TA_0^2} = \frac{\hbar\omega_0 e^{2g_{max}x}}{4A_0^2\sqrt{2\pi|\beta_2|x}},$$

where the factor of 2 takes into account that there are two sidebands.

The ratio of the energy in the $(n-1)$th harmonic to the energy in the pump beam can then be written as

$$2\frac{\int d\delta\, P_n(\omega_{max}+\delta)}{TA_0^2} = 2\eta^n n!\,|c_n|^2$$

which shows that up to the factor $2n!\,|c_n|^2$ the intensity in the $(n-1)$th harmonic is proportional to η^n. In our computation we assumed that each successive harmonic is smaller than the preceding ones, i.e., $P_n < P_{n-1}$. This allowed us to neglect the back action of higher order harmonics on lower order ones. Obviously this corresponds to the condition $\eta \ll 1$.

The above analysis does not provide an exact solution of the nonlinear Schrödinger equation (4). Rather we have only solved the linearized equation of Hasegawa and Brinkman, Eq. (5). Thus our main prediction Eq. (16) cannot be exact. We expect that the growth rate and spectral widths of the harmonics are robust predictions because they depend only on the fact that the $(n-1)$th harmonic is proportional to ϵ^n. On the other hand the prefactor, and in particular the value of the coefficients $|c_n|^2$, cannot be predicted correctly in the present approach. [Indeed by using as ansatz a nonlinear function different from Eq. (3), all our results would be unchanged except the coefficients c_n which would change.] Nevertheless the simple ansatz Eq. (3) gives surprisingly good predictions for the intensities (see the experimental results reported in Sec. III).

Let us conclude by sketching how one could carry out a more systematic approach to the harmonics of the MI that would predict correctly the prefactor of Eq. (16). Its starting point is the standard approach of the NLSE based on the linear equations described in Appendix A. There we took an ansatz of the form $A=(A_0+A_1)e^{i\phi_{NL}}$ and linearized the equations in A_1 to obtain Eq. (A1). But this is only an approximate solution. We can take into account systematic corrections to this solution by considering the ansatz $A=(A_0+A_1+A_2)e^{i\phi_{NL}}$ where A_1 is the solution of the linearized equations. One then obtains for A_2 the equation

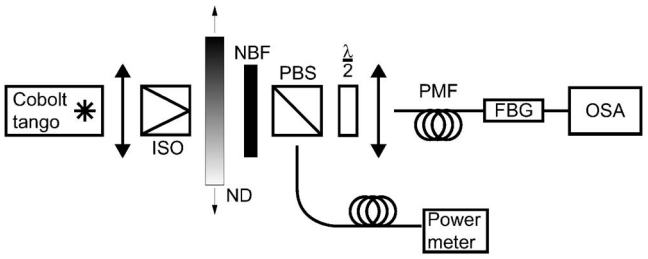

FIG. 1. Experimental setup. ISO, isolator; ND, variable neutral density filter; NBF, narrowband filter; PBS, polarizing beam splitter; λ/2, half-wave plate; PMF, polarization maintaining fiber; FBG, fiber Bragg grating; and OSA, optical spectrum analyzer.

$$i\partial_x A_2 = \frac{\beta_2}{2}\partial_\tau^2 A_2 - \gamma A_0^2(A_2 + A_2^*) - \gamma A_0(2|A_1|^2 + A_1^2).$$

This is a linear equation for A_2 with an independent term. Thus the solution of the equation for A_2 is a solution of the homogeneous equation plus a particular solution of the inhomogeneous equation. The independent term is quadratic in A_1 and therefore is proportional to $e^{2g_{max}x}$ and contains frequencies around $2\omega_{max}$ and around $\omega=0$. Upon solving for A_2 one will find that A_2 is largest around $2\omega_{max}$ and around $\omega=0$ and is proportional to $e^{2g_{max}x}$. Thus A_2 will encode the behavior of the second and zeroth harmonic. Successive orders in perturbation theory will give rise to the successive harmonics. We leave the detailed investigation of this approach to future work.

III. EXPERIMENTAL RESULTS

Our experimental setup is reported in Fig. 1. It consists of a Q switched laser (Cobolt Tango) that produces pulses at 1536 nm, with a 3.55 ns full width at half maximum duration T and a 2.5 kHz repetition rate f. The pump power $P_0=A_0^2$ is adjusted using a variable neutral density filter. A narrowband filter allows a wide spectral range around the pump wavelength to be free of noise. A polarizing beam splitter ensures that the pump is linearly polarized and allows measurement of the injected power proportional to the rejected beam. We used the Fibercore HB1250P polarizing maintaining fiber, although the experiment could equally have been realized with nonbirefringent fiber. A half-wave plate is used to ensure that the pump polarization is aligned with a principal axis of the fiber, whereupon polarization effects can be neglected and the above results for scalar MI apply. The fiber parameters are deduced from both scalar and vector modulation instabilities (see Ref. [10]). The fiber length L is 51 m. The group velocity dispersion parameter β_2 is $-15.27\ \mathrm{ps^2\,km^{-1}}$. The Kerr nonlinearity parameter γ is $3.26\ \mathrm{W^{-1}\,km^{-1}}$. (The beat length, which is irrelevant to the present experiment, is 17.9 mm.) Last, a fiber Bragg grating (FBG) rejects the pump wavelength before the measurement of the spectra. The rejection of the pump avoids detector blinding and allows us to reach the sensibility limit of the optical spectral analyzer (OSA).

The narrowband filter eliminates all residual photons except those at the pump wavelength. This ensures that the MI

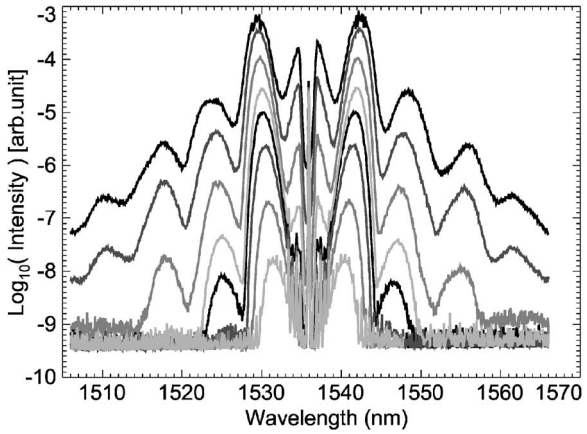

FIG. 2. Spectra of the output field for increasing peak power P_0 equal to 31.6, 38.9, 45.9, 49.1, 52.2, 57.4, 59.6, and 62.4 W. The resolution bandwidth is 0.1 nm. Note that the fiber Bragg grating has removed the pump wavelength, thereby avoiding detector blinding and allowing us to reach the sensitivity limit of the OSA.

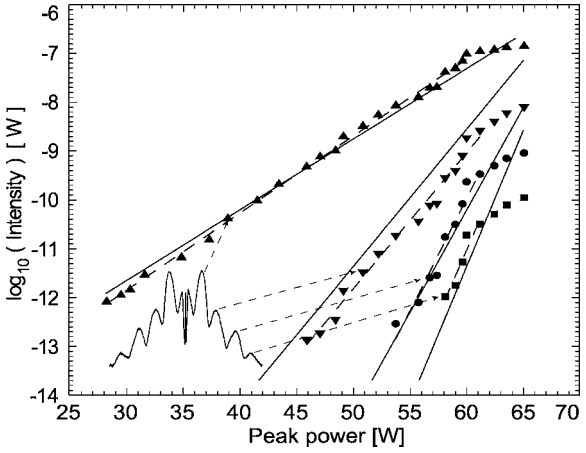

FIG. 3. Maximum intensity as a function of the peak power of the pump. The up triangles, down triangles, circles, and squares represent, respectively, the fundamental MI peak ($n=1$), and the first ($n=2$), second ($n=3$), and third ($n=4$) harmonics. The dashed lines are a fit to the data according to an exponential law. The continuous curves are the theoretical predictions of Eq. (16). As described in the text the experimental points were shifted by 7 dB to agree with the theoretical predictions. For clarity, we show a spectrum.

and harmonics indeed arise from vacuum fluctuations and not from classical noise. We have checked that this is indeed the case in two ways. First numerical simulations of the stochastic nonlinear Schrödinger equation reproduce very well the observed spectra, including the harmonics [10]. Second we have studied in detail, using a single photon detector, the MI in the regime where relatively few photons are produced. This investigation shows that there is in fact a small amount of noise present due to spontaneous Raman scattering in the fiber. But the number of Raman photons per mode is much smaller than 1 which means that they do not affect the spectra when the gain is large. In summary both investigations show that the MI process is dominated by spontaneous effects and stimulation by classical noise is negligible.

A sample of the collected spectra is shown in Fig. 2 for different pump powers P_0. We clearly observe the growth of the MI and the appearance and growth of the harmonics as the pump power increases. The largest pair of peaks correspond to the MI. Then each new harmonic gives rise to a pair of peaks further and further from the pump wavelength. In addition there is a peak around the pump wavelength. Because this peak overlaps with the pump it is largely rejected by the FBG and cannot be well characterized from this first set of measurements. In consequence we have characterized the peak around the pump wavelength from a second set of measurements obtained without the FBG (figure not shown). For each pump power P_0, each harmonic has been fitted according to a Gaussian function $I_n(P_0)\exp\{-[\omega-\omega_n(P_0)]^2/2\sigma_n^2(P_0)\}$ where I_n, ω_n, and σ_n characterize the intensity, frequency, and spectral width of the harmonic.

The measured intensities $I_n(P_0)$ of each harmonic are compared in Fig. 3 to the theoretical predictions (continuous curve). To obtain the theoretical curves, Eq. (16) must be integrated over the OSA resolution bandwidth (0.1 nm). Moreover we must identify $\delta(0)=T\times S\times f/2\pi N_s$, where T is the pulse full width at half maximum, S is the sweep time equal to 27.9 s, f is the laser repetition rate, and N_s denotes the number of samples per spectrum equal to 1001. In order to obtain a good overlap between theoretical curves and measured points, we had to further shift $\delta(0)$ by 7 dB. This discrepancy is not unreasonable given that the above theory was based on a continuous pump, whereas now we are dealing with a Gaussian pulse, and given our inability to carry out absolute measurements with the OSA. With this shift the theoretical and experimental intensities agree well. This shows that Eq. (16), including both the exponential terms and the prefactor, correctly predicts the absolute intensities of the harmonics. We further confirmed this agreement by fitting the intensity of each harmonic to an exponential law $I_n(P_0)\simeq A_n\exp(\alpha_n 2\gamma P_0 L)$ where A_n is an n dependent constant, and α_n a growth factor (dotted lines in Fig. 3). Theory predicts that $\alpha_n/\alpha_1=n$. This prediction is well verified (see Table I).

Note that around 60 W the total energy in the sidebands becomes comparable with the pump energy: the MI saturates and our analysis is no longer valid.

TABLE I. Behavior of the harmonics. The theoretical prediction is that all the quantities are equal to n (except the center frequency of the second harmonic centered on $\omega=0$).

n(order of harmonic$=n-1$)	Measured values		
	$\langle\sigma_n^2/\sigma_1^2\rangle_{P_0}$	$\langle\omega_n/\omega_1\rangle_{P_0}$	α_n/α_1
$2(\omega\simeq 0)$	2.11 ± 0.03[a]	0[a]	2.43 ± 0.15[a]
$2(\omega\simeq 2\omega_{max})$	2.31 ± 0.02[a]	1.95 ± 0.01[a]	1.99 ± 0.12[a]
$2(\omega\simeq 2\omega_{max})$	2.15 ± 0.07[b]	1.85 ± 0.01[b]	1.77 ± 0.06[b]
3	2.21 ± 0.06[b]	2.95 ± 0.01[b]	2.92 ± 0.23[b]
4	4.89 ± 0.15[b]	3.94 ± 0.03[b]	3.36 ± 0.61[b]

[a]Second set of measures.
[b]First set of measures.

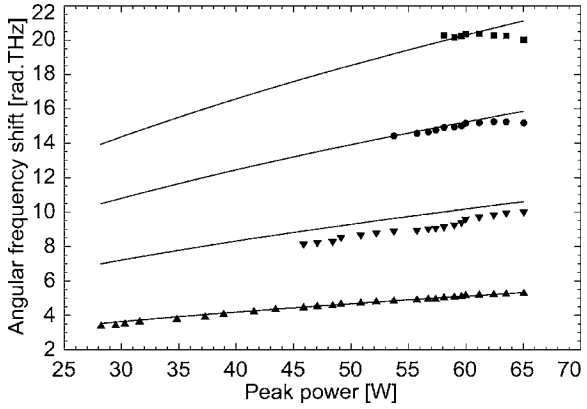

FIG. 4. Angular frequency shift as a function of the peak power P_0 of the pump. The up triangles, down triangles, circles, and squares represent, respectively, the fundamental MI peak ($n=1$), and the first ($n=2$), second ($n=3$), and third ($n=4$) harmonics. The continuous curves correspond to the theoretical prediction $\omega_n = n\sqrt{2\gamma P_0/|\beta_2|}$.

Theory predicts that the harmonic around $\omega=0$ should have the same growth rate, but four times the intensity, as the harmonic around $2\omega_{max}$. There is reasonable agreement concerning the growth rate (see Table I). We were unable to check the factor of 4 as the intensity measurements of the harmonic around $\omega=0$ were not precise enough, although it is always more intense than the harmonic around $2\omega_{max}$ (see Fig. 2).

We now turn to the angular frequency shifts $\omega_n(P_0)$. In Fig. 4 we plot the measured values and the theoretical predictions (continuous curves). We note a very good overlap. Moreover, from the data in Fig. 4, we have computed the ratios between the $(n-1)$th harmonic frequency $\omega_n(P_0)$ and the fundamental frequency $\omega_1(P_0)$. The average values $\langle \omega_n/\omega_1 \rangle_{P_0}$ (where the average is over the different values of P_0) are reported in Table I. There is good agreement with the theoretical prediction $\omega_n/\omega_1 = n$.

Finally, the measured spectral widths σ_n are reported in Fig. 5 as a function of P_0. They are compared to the theoretical values $\sqrt{n/4|\beta_2|L}$ (straight lines). The agreement is good for the fundamental frequency ($n=1$) and the first harmonic ($n=2$). In the case of the second ($n=3$) and third ($n=4$) harmonics it is not possible to draw a conclusion, although the values are consistent with an increase in spectral width with the order of the harmonic. This is because for high pump powers (>60 W) the MI saturates; in this regime we find that the spectral width increases for all values of n. And when the peaks of the MI harmonics have low intensity they are broadened for an unknown reason. For the second ($n=3$) and third ($n=4$) harmonics the widths are always affected by one of these effects. Finally, the ratios $\langle \sigma_n^2/\sigma_1^2 \rangle_{P_0}$ (where the average is taken over those values of P_0 where σ_n is approximately constant) are reported in Table I. As expected, only the first harmonic leads to a proper value.

IV. CONCLUSION

In summary we have studied the higher order harmonics of modulational instability in the regime where the MI arises spontaneously through amplification of vacuum fluctuations. We have shown that in this regime there is a rich phenomenology which can be predicted theoretically and is well verified experimentally. In particular we have obtained predictions for the detunings, intensities, growth rates, and spectral widths of the harmonics [see our key result Eq. (16)]; and found good agreement with our experimental results based on light propagation in optical fibers. We note that the shape of the spectrum, and in particular the relative intensities of the higher order harmonics, is highly sensitive to the initial presence of classical noise, and can therefore be taken as a signature that the MI is seeded by vacuum fluctuations. It should be possible to extend our work in a number of directions, for instance to predict exactly the coefficients $|c_n|^2$ appearing in Eq. (16), to study the regime where the pump starts to get depleted, and to extend it to other forms of MI, or to other kinds of instabilities.

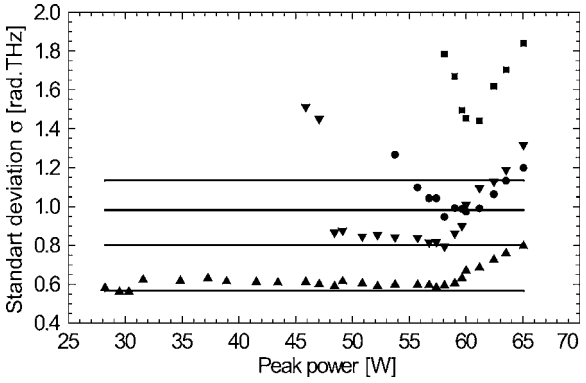

FIG. 5. The spectral width σ_n of each harmonic is shown as a function of the peak intensity P_0. The up triangles, down triangles, circles, and squares represent, respectively, the fundamental MI peak, and the first, second, and third harmonics. Straight lines correspond to the theoretical prediction $\sigma_n = \sqrt{n/4|\beta_2|L}$.

ACKNOWLEDGMENTS

This research was supported by the Interuniversity Attraction Poles Program—Belgium Science Policy—under Grant No. V-18, by the Action de Recherche Concertée de la Communauté Française de Belgique, and by the Fonds Defay.

APPENDIX A: MODULATIONAL INSTABILITY

In this appendix we recall the usual approach to MI. We first solve the linearized equations, then consider the predictions of quantum theory, and finally consider the regime of large gain. This appendix thus contains background material useful for reading the rest of the article.

1. Linear perturbation theory

In order to solve the NLSE Eq. (1) we consider an ansatz of the form

$$A = (A_0 + A_1)e^{i\phi_{NL}},$$

where A_1 is a small perturbation. We linearize the NLSE around the continuous solution to obtain the equation for A_1:

$$i\partial_x A_1 = \frac{\beta_2}{2}\partial_\tau^2 A_1 - \gamma A_0^2(A_1 + A_1^*). \tag{A1}$$

We then carry out a Fourier expansion of A_1:

$$A_1(\tau,x) = \frac{1}{\sqrt{2\pi}}\int d\omega\, a_1(x,\omega)e^{-i\omega\tau}, \tag{A2}$$

where ω is the detuning with respect to ω_0. Equation (A1) then becomes

$$i\partial_x a_1(x,\omega) = -\frac{\beta_2}{2}\omega^2 a_1(x,\omega) - \gamma A_0^2[a_1(x,\omega) + a_1^*(x,-\omega)]. \tag{A3}$$

When $\beta_2 < 0$ and when $0 \leqslant \omega^2 \leqslant \omega_c^2 = 4\gamma A_0^2/|\beta_2|$ this equation possesses exponentially growing and exponentially decreasing solutions. On the other hand when $\omega^2 > \omega_c^2$ or when $\beta_2 > 0$ Eq. (A3) possesses oscillating solutions. Let us consider the unstable solutions. These are proportional to $e^{\pm gx}$ where the gain is

$$g = \frac{|\beta_2\omega|}{2}\left(\frac{4\gamma A_0^2}{|\beta_2|} - \omega^2\right)^{1/2}. \tag{A4}$$

We can reexpress the solution in terms of the initial conditions as

$$a_1(x,\omega) = a_1(0,\omega)\mu(x,\omega) + a_1^*(0,\omega)\nu(x,\omega), \tag{A5}$$

$$\mu(x,\omega) = \cosh(gx) + i\frac{(\gamma A_0^2 + \beta_2\omega^2/2)}{g}\sinh(gx), \tag{A6}$$

$$\nu(x,\omega) = i\frac{\gamma A_0^2}{g}\sinh(gx), \tag{A7}$$

where μ and ν obey the condition $|\mu|^2 - |\nu|^2 = 1$.

2. Quantum theory

The above solution of the NLSE can also be used to derive the form of the instability when the modulational instability is seeded by vacuum fluctuations. In this case Eq. (1) should be interpreted as the Heisenberg equation for the operators $\hat{A}$ and $\hat{A}^\dagger$. The Fourier transform Eq. (A2) defines the destruction operators $\hat{a}_1(x,\omega)$. Their Hermitian conjugates $\hat{a}_1^\dagger(x,\omega)$ are the creation operators. These operators obey the commutation relations

$$[\hat{a}_1(x,\omega), \hat{a}_1^\dagger(x,\omega')] = \hbar(\omega_0 + \omega)\delta(\omega - \omega'). \tag{A8}$$

Equation (A5) should then be reinterpreted as giving the relation between the creation and destruction operators at distance x along the fiber and at the origin $x=0$:

$$\hat{a}_1(x,\omega) = \hat{a}_1(0,\omega)\mu(x,\omega) + \hat{a}_1^\dagger(0,\omega)\nu(x,\omega). \tag{A9}$$

The initial state $|0\rangle$ contains no photons:

$$\hat{a}_1(0,\omega)|0\rangle = 0. \tag{A10}$$

From Eq. (A9) one can then compute the expectation values of products of creation and destruction operators at distance x along the fiber. For instance one finds

$$\langle 0|\hat{a}_1^\dagger(x,\omega)\hat{a}_1(x,\omega')|0\rangle = \hbar(\omega_0 - \omega)|\nu(x,\omega)|^2\delta(\omega - \omega'). \tag{A11}$$

From this it follows that the spectral power density at frequency $\omega_0+\omega$, $P(x,\omega)$, is given by

$$P(x,\omega) = \langle 0|\hat{a}_1^\dagger(x,\omega)\hat{a}_1(x,\omega)|0\rangle = \hbar(\omega_0 - \omega)|\nu(x,\omega)|^2\delta(0) \simeq \hbar\omega_0|\nu(x,\omega)|^2\delta(0). \tag{A12}$$

It is infinite because we have computed the power when the pump beam is monochromatic and of infinite duration. If we suppose that the pump beam lasts only for a duration T then one should—as usual in these kinds of situations—interpret this infinity as

$$\delta(0) \equiv \frac{T}{2\pi}. \tag{A13}$$

Then the spectral power density at position x at frequency $\omega_0+\omega$ is $P(x,\omega) = \hbar\omega_0|\nu|^2 T/2\pi$.

Note that the quantum solution also predicts other effects such as correlations (two-mode squeezing) which will not be studied here.

3. Behavior in the regime of large gain

We now consider the regime where the gain e^{gx} is large. In this case we can simplify the solutions obtained above. First of all we note that the produced photons will be localized around the frequency ω_{max} at which the gain is maximum:

$$\omega_{max}^2 = \frac{2\gamma A_0^2}{|\beta_2|}. \tag{A14}$$

The maximum gain is given by

$$g_{max} = g(\omega_{max}) = \gamma A_0^2. \tag{A15}$$

In order to describe the behavior in the vicinity of the maximum gain we can expand the gain around ω_{max} as

$$g(\omega) \simeq g_{max} - \frac{g''}{2}(\omega - \omega_{max})^2, \tag{A16}$$

where $g'' = 2|\beta_2|$. In the vicinity of ω_{max} the coefficients μ and ν simplify. They can be approximated by

$$\mu(x,\omega) \simeq \frac{1}{2}\exp[xg_{max} - xg''/2(\omega - \omega_0)^2],$$

$$\nu(x,\omega) \simeq \frac{i}{2}\exp[xg_{max} - xg''/2(\omega - \omega_0)^2],$$

where we have kept only the exponentially growing terms in μ, ν, used the approximate expressions derived in Eq. (A16) and dropped the ω dependence of the prefactors in μ, ν.

Furthermore in the regime of large gain the quantum solution simplifies. Indeed, since there are many photons in each mode one can carry out a semiclassical treatment in which one neglects ordering problems. Thus in this regime

one can reproduce the predictions of the quantum solution by taking the initial conditions of the classical solution $a(0,\omega)$ to be white noise with power $\hbar\omega_0/2$ per mode. More precisely the $a(0,\omega)$ should be taken to be complex δ correlated Gaussian random variables distributed according to the probability distribution

$$P(a(0,\omega)) = \frac{1}{2\pi\sigma^2} e^{-|a|^2/2\sigma^2}, \tag{A17}$$

with variance σ^2 such that

$$\langle a(0,\omega) a^*(0,\omega')\rangle = \frac{\hbar\omega_0}{2}\delta(\omega-\omega'). \tag{A18}$$

This will correctly reproduce the quantum predictions up to corrections proportional to $\exp(-gx)$. Indeed, taking the probability distribution to be Gaussian correctly reproduces in the regime of large gain the combinatorial factors which arise from Wick contractions when expectation values of the products of many creation and destruction operators are taken. Thus for instance in this regime we have

$$\langle a(0,\omega_1)\cdots a(0,\omega_n) a^*(0,\omega_1')\cdots a^*(0,\omega_m')\rangle = \frac{(\hbar\omega_0)^n}{2^n}\delta_{n,m}\sum_\sigma \delta(\omega_1-\omega'_{\sigma(1)})\cdots\delta(\omega_n-\omega'_{\sigma(n)}), \tag{A19}$$

where the sum is carried out over all permutations σ of $\{1,\ldots,n\}$.

In the regime of large gain the spectral power density is thus

$$P(x,\omega) = \langle a^*(x,\omega) a(x,\omega)\rangle = \frac{T}{2\pi}\frac{\hbar\omega_0}{4}\exp(2g_{max}x)\exp[-g''(\omega-\omega_{max})^2 x]. \tag{A20}$$

APPENDIX B: DETAILS OF CALCULATIONS

1. Relation between ϵ, σ, and a

Upon linearizing Eq. (3) in ϵ and σ we obtain

$$A = A_0 e^{i\phi_{NL}}(1+\epsilon/2+i\sigma).$$

Upon inserting the forms given by Eqs. (6) and (7) one finds

$$A = A_0 e^{i\phi_{NL}}\left[1+\frac{1}{\sqrt{2\pi}}\int_0^\infty d\omega \times \epsilon_+(\omega)\left(\frac{1}{2}+\frac{ig}{|\beta_2|\omega^2}\right)e^{-i\omega\tau+gx} + \epsilon_-(\omega)\left(\frac{1}{2}-\frac{ig}{|\beta_2|\omega^2}\right)e^{-i\omega\tau-gx} + \epsilon_+^*(\omega)\left(\frac{1}{2}+\frac{ig}{|\beta_2|\omega^2}\right) \times e^{+i\omega\tau+gx} + \epsilon_-^*(\omega)\left(\frac{1}{2}-\frac{ig}{|\beta_2|\omega^2}\right)e^{+i\omega\tau-gx}\right].$$

We can then identify

$$\epsilon_+(\omega) = \frac{a_1(0,\omega)}{2A_0}\left(1-i\frac{|\beta_2|\omega^2}{2g}\right)+\frac{a_1^*(0,\omega)}{2A_0}\left(1+i\frac{|\beta_2|\omega^2}{2g}\right),$$

$$\epsilon_-(\omega) = \frac{a_1(0,\omega)}{2A_0}\left(1+i\frac{|\beta_2|\omega^2}{2g}\right)+\frac{a_1^*(0,\omega)}{2A_0}\left(1-i\frac{|\beta_2|\omega^2}{2g}\right), \tag{B1}$$

which in the regime of large gain reduces to Eq. (12).

2. Power spectrum of the harmonics

Here we give the details of the calculations leading from Eq. (15) to Eq. (16). If we make Eq. (15) explicit we obtain

$$A_n(x,\tau) = c_n A_0 e^{i\phi_{NL}}\epsilon^n = \frac{c_n A_0 e^{i\phi_{NL}}}{(2\pi)^{n/2}}\int_{\omega_j\simeq\omega_{max}}\prod_{j=1}^n d\omega_j \times\exp\left(-i\sum_{j=1}^n\omega_j\tau\right)\exp\left(\sum_{j=1}^n g(\omega_j)x\right) \times\prod_{j=1}^n\left(\frac{a_{\omega_j}}{A_0}\frac{1-i}{2}+\frac{a^*_{-\omega_j}}{A_0}\frac{1+i}{2}\right), \tag{B2}$$

where for conciseness we denote $a_\omega = a_1(0,\omega)$. This term contains frequencies around: $-n\omega_{max}$, $-(n-2)\omega_{max}$, …, $(n-2)\omega_{max}$, $n\omega_{max}$.

The only new frequencies that appear at order n are thus around $\pm n\omega_{max}$ (except for $n=2$ when new frequencies appear also around $\omega=0$). It is the behavior of the nth order term around these frequencies that we are interested in.

We thus take the Fourier component of $c_n e^{i\phi_{NL}}A_0\epsilon^n$ at frequency $n\omega_{max}+\delta$ to obtain

$$A_n(x,n\omega_{max}+\delta) = \frac{c_n A_0 e^{i\phi_{NL}}}{(2\pi)^{(n-1)/2}}\int_{\omega_j\simeq\omega_{max}}\prod_{j=1}^n d\omega_j \times\delta\left(\sum_{j=1}^n\omega_j - n\omega_{max}-\delta\right)\exp\left(\sum_{j=1}^n g(\omega_j)x\right) \times\prod_{j=1}^n\left(\frac{a_{\omega_j}}{A_0}\frac{1-i}{2}+\frac{a^*_{-\omega_j}}{A_0}\frac{1+i}{2}\right). \tag{B3}$$

The spectral density of power at frequency $n\omega_{max}+\delta$ is

$$P_n(n\omega_{max}+\delta) = \langle|A_n(n\omega_{max}+\delta)|^2\rangle = \frac{|A_0|^2|c_n|^2}{(2\pi)^{n-1}}\frac{(\hbar\omega_0)^n}{2^n|A_0|^{2n}}\int\prod_{j=1}^n d\omega_j\prod_{j=1}^n d\omega_j' \times\delta\left(\sum_{j=1}^n\omega_j - n\omega_{max}-\delta\right) \times\delta\left(\sum_{j=1}^n\omega_j' - n\omega_{max}-\delta\right)$$

$$\times \exp\left(\sum_{j=1}^{n} (g(\omega_j) + g(\omega_j')x)\right)$$

$$\times \frac{1}{2^n}\sum_{\sigma} 2\delta(\omega_1 - \omega_{\sigma(1)}') \cdots 2\delta(\omega_n - \omega_{\sigma(n)}'), \tag{B4}$$

where the sum over σ is a sum over all $n!$ possible permutations. Carrying out the integrals over ω_j' this becomes

$$P_n(n\omega_{max} + \delta) = \delta(0)\frac{|A_0|^2|c_n|^2}{(2\pi)^{n-1}}\frac{(\hbar\omega_0)^n n!}{2^n|A_0|^{2n}}\int \prod_{j=1}^{n} d\omega_j \times \delta\left(\sum_{j=1}^{n}\omega_j - n\omega_{max} - \delta\right)\exp\left(2\sum_{j=1}^{n} g(\omega_j)x\right). \tag{B5}$$

To evaluate the remaining integral we make the change of variables

$$\omega_j = \omega_{max} + \frac{\delta}{n} + \xi_j.$$

In terms of these variables we have

$$2\sum_{j=1}^{n} g(\omega_j) = 2ng_{max} - g''\frac{\delta^2}{n} - g''\sum_{j=1}^{n}\xi_j^2$$

(since $\Sigma_{j=1}^{n}\xi_j = 0$). We recall that g'' is equal to $2|\beta_2|$. We thus have

$$\int \prod_{j=1}^{n} d\omega_j \delta\left(\sum_{j=1}^{n}\omega_j - n\omega_{max} - \delta\right)\exp\left(2\sum_{j=1}^{n} g(\omega_j)x\right) = \exp(2ng_{max}x)\exp(-g''\delta^2 x/n)\int \prod_{j=1}^{n} d\xi_j \delta\left(\sum_{j=1}^{n}\xi_j\right) \times \exp\left(-g''\sum_{j=1}^{n}\xi_j^2 x\right) = \frac{1}{\sqrt{n}}\left(\frac{\sqrt{\pi}}{\sqrt{g''x}}\right)^{n-1}\exp(2ng_{max}x) \times \exp(-g''x\delta^2/n), \tag{B6}$$

where the integral over ξ_j is carried out as follows. Change variables to $\zeta_j = \Sigma_k R_{jk}\xi_k$ where R is an orthogonal matrix such that $\zeta_1 = \Sigma_k \xi_k/\sqrt{n}$. Then the Jacobian of this transformation is 1. The integrals over ζ_j factorize into one δ function and $n-1$ Gaussians, yielding Eq. (B6). Inserting this into Eq. (B5) yields Eq. (16).

[1] T. B. Benjamin and J. E. Freir, J. Fluid Mech. **27**, 417 (1967).

[2] T. Taniuti and H. Washimi, Phys. Rev. Lett. **21**, 209 (1968); A. Hasegawa, *ibid.* **24**, 1165 (1970).

[3] L. A. Ostrovskii, Sov. Phys. JETP **24**, 797 (1969).

[4] A. Hasegawa and W. F. Brinkman, IEEE J. Quantum Electron. **16**, 694 (1980).

[5] K. Tai, A. Hasegawa, and A. Tomita, Phys. Rev. Lett. **56**, 135 (1986).

[6] G. P. Agrawal, *Nonlinear Fiber Optics*, 3rd. ed., (Academic Press, San Diego, 2001).

[7] L. Salasnich, A. Parola, and L. Reatto, Phys. Rev. Lett. **91**, 080405 (2003).

[8] N. N. Akhmediev and V. I. Korneev, Theor. Math. Phys. **69**, 1089 (1986)

[9] G. Van Simaeys, Ph. Emplit, and M. Haelterman, Phys. Rev. Lett. **87**, 033902 (2001).

[10] D. Amans, E. Brainis, Ph. Emplit, M. Haelterman, and S. Massar, Opt. Lett. **30** 1051 (2005).